Critical current of grain boundaries in $YBa_2Cu_3O_x$ bicrystal films as a function of oxygen concentration

H. Claus,[1,2] Beihai Ma,[3] A. P. Paulikas,[1] R. Nikolova,[1,*] B. W. Veal,[1] Q. X. Jia,[4] U. Welp,[1] and K. E. Gray[1]
[1]*Materials Science Division, Argonne National Laboratory, Argonne, Illinois 60439, USA*
[2]*Department of Physics, University of Illinois at Chicago, Chicago, Illinois 60607-7059, USA*
[3]*Energy Systems Division, Argonne National Laboratory, Argonne, Illinois 60439, USA*
[4]*Superconductivity Technology Center, Los Alamos National Laboratory, Los Alamos, New Mexico 87545, USA*
(Received 29 November 2006; revised manuscript received 16 April 2007; published 27 July 2007)

The effect of oxygen doping on the critical current density J_C across [001] tilt grain boundaries in $YBa_2Cu_3O_x$ thin films, epitaxially grown on bicrystal substrates, is investigated. Grain boundary misorientations were varied between 0° and 24°. It is observed that for 24° grain boundaries, the critical current enhancement due to oxygen overdoping can be as large as a factor of 10 when compared to J_C at optimal doping (where T_C is maximum). This oxygen-induced enhancement of the grain boundary J_C is similar to that observed with optimized Ca doping. For 15° and 10° grain boundaries, the relative enhancement due to oxygen doping is smaller than that of the 24° grain boundary. It is observed that the grain boundaries often degrade after repeated oxygen treatments, most likely because of chemical contamination. Much larger enhancements in the grain boundary critical current densities might be achievable with heavy oxygen doping if this competing degradation could be avoided. The critical current is determined using a contact-free magnetic method which measures the maximum current that can be induced by an external field in a ring sample. For a 24° grain boundary, we demonstrate that the critical current determined by the magnetization method is in excellent agreement with J_C obtained from transport measurements.

DOI: 10.1103/PhysRevB.76.014529 PACS number(s): 74.25.Sv, 74.25.Ha, 74.62.Dh

I. INTRODUCTION

Most high-angle grain boundaries (GBs) in high-temperature superconductors exhibit[1] notoriously low critical current densities J_C. This difficulty[2] has led to several ingenious methods[3–5] to reduce the mosaic spread of GB angles in coated conductors. However, these add to the complexity of fabrication and place severe demands on quality control to produce long lengths of coated conductors with $J_C > 1$ MA/cm^2 at 77 K. In another approach, it was recently shown that Ca doping of $YBa_2Cu_3O_x$ (YBCO) GBs can yield impressive improvements in supercurrent transport[6,7] across 24° GBs. However, Ca doping of YBCO films reduces their superconducting transition temperature T_C by more than 10 K, from above 90 K for the undoped material to about 80 K for 30% Ca doping.[6,7]

In this paper, an alternative approach for improving the GB J_C based on oxygen overdoping is systematically studied in [001] tilt GBs with angles of 0°–24° that are made by epitaxial growth of YBCO onto $SrTiO_3$ bicrystal substrates.[8] The results strongly suggest that the maximum GB J_C is achieved with significant oxygen overdoping. Note that oxygen overdoping also reduces T_C of the film defining the GB, but in this case by less than 5 K as compared with 10 K seen in Ca doping. For a 24° GB, with oxygen overdoping we have observed a factor of 10 improvement in J_C compared with the "as-made" sample. The as-made condition refers to a standard preparation procedure which leaves the sample nearly optimally doped (maximum T_C). This oxygen-induced enhancement is similar to the enhancement reported for Ca doping of a 24° bicrystal GB.[6] For 10° and 15° GBs, relative improvements in J_C resulting from enhanced oxygenation were smaller (although absolute improvements in J_C increased as the GB angle became smaller).

Importantly, our contact-free technique allows for sequential reprocessing at high temperatures without any foreign materials that would be needed for contacts in transport measurements. Nevertheless, in some cases, J_C values degrade after repeated oxygenation. The root cause of this degradation is not yet fully understood and needs clarification. It may be caused by chemical contamination.

This work is an extension of an earlier study of oxygen doping of coated conductor films.[9] That work demonstrated that J_C systematically increases as the level of oxygen doping increases even though T_C decreases in the overdoped condition. Here, we examine the behavior of critical current densities across grain boundaries and the dependence of the GB J_C on the level of oxygen doping and discuss possible origins of the similar behavior of GBs and intragranular J_C.

II. EXPERIMENT

Bicrystal films of YBCO were grown on commercial $SrTiO_3$ bicrystal substrates (Superconductive Components, Columbus, OH) by pulsed laser deposition (PLD) using a Lambda Physik LPX 210i excimer laser, with $Kr-F_2$ gas premixture as the lasing medium. The experimental setup of our PLD system was reported earlier.[10] This PLD system has an optical beam raster to produce films with better uniformity over a broader area. The laser beam is focused at the target through a quartz lens (1000 mm focal length) coated with antireflective coating and is reflected by a mirror that is mounted as part of the beam raster. The reflected beam hits a rotating YBCO target at a 45° incident angle. The target carousel can carry up to four 2 in. in diameter targets to accommodate the needs for multiple layer ablation without breaking vacuum.

Commercial targets (Superconductive Components, 99.999% pure), 45 mm in diameter and 6 mm in thickness, were used. Substrates were attached to a heatable sample stage with silver paste and heated to a high temperature (700–800 °C) during deposition. The base pressure of the PLD chamber was $\approx 1 \times 10^{-5}$ Torr. The desired operating pressure (≈200 mTorr) was maintained by flowing ultrahigh-purity oxygen at ≈10 SCCM (SCCM denotes cubic centimeter per minute at STP) and pumping the chamber with a molecular turbopump. The size of the laser spot focused at the rotating target was ≈12 mm^2, which produced an energy density of ≈2.0 J/cm^2. The distance between the target and the substrates was ≈7 cm.

In situ oxygen annealing was carried out inside the PLD chamber on as-grown YBCO bicrystal films. After deposition, the sample, along with the heater, was rapidly cooled to 450 °C at ≈50 °C/min. Then, the chamber was back-filled with ultrahigh purity oxygen to pressure of ≈700 Torr. The sample was kept for 1 h at 450 °C in the chamber before cooling to room temperature at ≈10 °C/min. This *in situ* annealing process in general leads to optimally doped (highest T_C) PLD YBCO films. The film thickness was about 200 nm.

After deposition, rings of dimensions of 4 mm outer diameter and 3 mm inner diameter were produced by photolithography, with the grain boundary bisecting the film ring. The cross sectional area of the rings are about 0.5 mm $\times 200$ nm$=10^{-6}$ cm^2.

For the study of supercurrent transport across GBs, we use the persistent-current magnetization technique.[9,11] When a magnetic field is applied to a superconducting ring, a supercurrent is induced in the ring that circulates around the ring to screen the magnetic field from the ring interior. The circulating current generates a magnetic moment that is proportional to the supercurrent. This technique was employed previously to investigate epitaxial film rings without GBs (Refs. 12 and 13) and also films with artificial GBs.[8,14] For small applied fields (<5 mT), our measurements were performed in a noncommercial superconducting quantum interference device (SQUID) magnetometer[11] and, at higher fields, in a commercial vibrating sample magnetometer (VSM). For one ring containing a 24° GB, we also determined J_C at 77 K by transport measurements.

For the secondary oxygenation of the films, we devised the following scheme. First, a container with a tight lid was fabricated from porous melt-textured YBCO. The oxygen concentration of the container was then fixed to that desired for the film by giving it the appropriate oxygenation treatment. This container then acts as a buffer to maintain the correct oxygen partial pressure for the entire temperature profile experienced by the film during annealing. Note that it takes about 2 weeks to fully oxygenate the container at 400 °C. The thin film was then placed inside the container and placed in the furnace under the exact same oxygenation condition the container was exposed to originally. The annealing time, sufficient for the film to come to equilibrium with the container, was between 1 h and 1 week, depending on the temperature. For example, at 300 °C, 3 h were sufficient to oxygenate the film. For each oxygenation temperature, chosen for the film rings, we prepared a separate container. After oxygenation of the films, the container with the ring sample inside was quenched into liquid nitrogen.

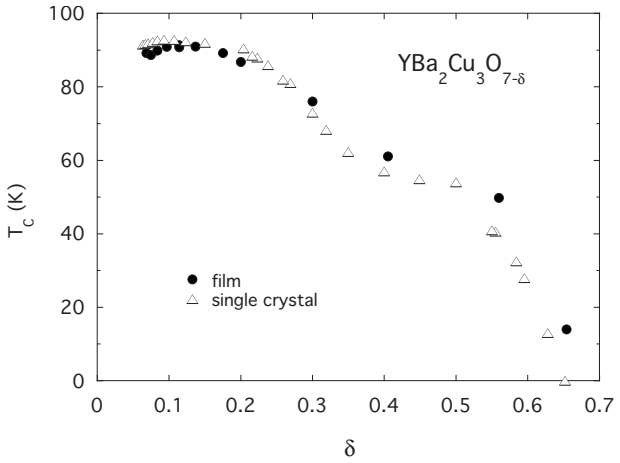

FIG. 1. Superconducting transition temperature of YBCO single crystals and epitaxial YBCO thin films. The oxygen concentration, $x=7-\delta$, of the film was taken to be the same as that of the melt-textured container (see text).

Most samples survived many secondary oxidation experiments without degradation, whereas some showed degradation after a few secondary anneals. After several anneals of a given sample, we attempted to reproduce the results obtained after the first anneal. If the results were not reproducible, we concluded that the sample had degraded and discarded it. To avoid this degradation we later changed the ring fabrication method for the film rings. After the YBCO deposition, the samples were covered with a protective Ag layer (about 0.5 μm thick). The samples were then covered with a ring mask. The uncovered part of the film was then removed by a miniature sand blaster.[9] In this work, all films containing GBs were made using photolithography. The single crystal film ring was made with the second method, involving sand blasting.

With our oxygenation technique, we were able to reversibly change the oxygen concentration of the film from the underdoped to the overdoped regime. Figure 1 displays the superconducting transition temperature of a single crystal film as a function of the oxygen concentration. For comparison, earlier data for single crystals are also shown.[15] These films were not subjected to photolithography (in contrast to the thin-film samples use for J_C determination, see below). The oxygen concentration of the film was assumed to be the same as that of the melt-textured container and was determined from a prior calibration of $x=7-\delta$ vs temperature and oxygen partial pressure obtained from studies of ceramic YBCO.[16] The fact that T_C vs oxygen concentration of the films follows closely that of the single crystals (Fig. 1) strongly suggests that our method of determining the oxygen concentration of our thin films is justified.

III. RESULTS AND DISCUSSION

A. As-made GBs

1. Low critical current measurements

In this section, we discuss results obtained on as-made film rings before they were subjected to the secondary oxy-

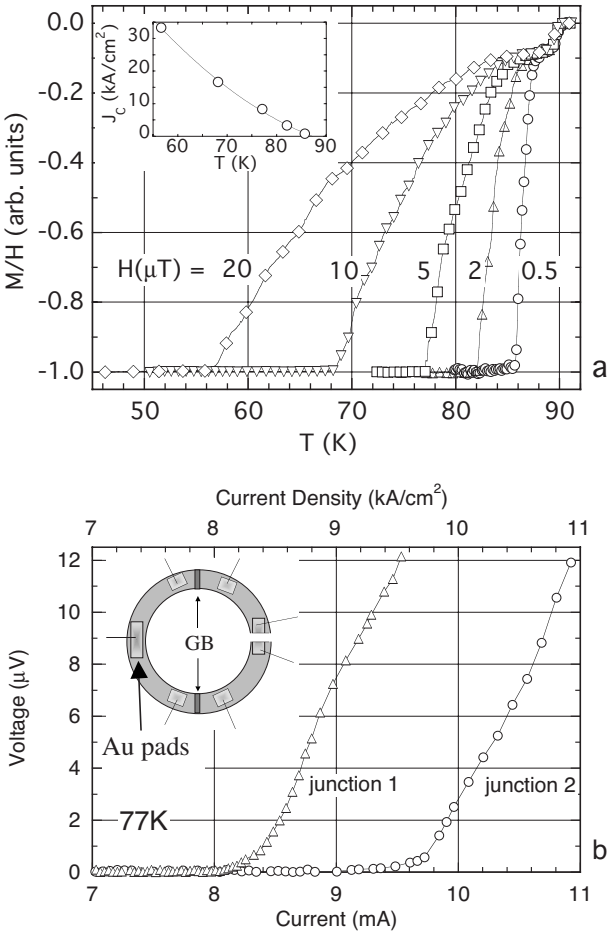

FIG. 2. (a) (Upper panel): Magnetic susceptibility of a ring containing a 24° GB in various fields. The data were obtained on warming after initially cooling in zero field to low temperatures. The inset show the critical current density obtained from the applied field and the corresponding kink temperatures (see text). (b) (Lower panel): Current-voltage characteristics of the two junctions contained in the same ring used in the upper panel. The upper scale shows the current density. The inset schematically shows the ring after leads were attached and a slit cut into it.

genation treatments. Figure 2(a) (upper panel) shows the magnetization (M), normalized to the applied field (H), measured vs temperature for an as-made ring containing a 24° [001] tilt GB. The measurements were taken on warming after initially cooling in zero field to low temperature where the indicated fields were applied. As the temperature increases, an abrupt increase in M/H appears (kink in M/H vs T) when the induced screening current exceeds the *grain boundary* critical current (which monotonically decreases with increasing temperature) and magnetic flux starts penetrating through the GB into the core of the ring.[11] At temperatures above the kink, the screening current decreases since it is limited by the temperature-dependent GB critical current and the magnitude of the diamagnetic signal decreases. A plateau in M versus T is reached when the critical current through the boundary has dropped to zero. The remaining signal is due to the diamagnetic signal of the YBCO film material in the annulus, equivalent to a ring with two slits.[11] The inset in Fig. 2(a) shows the temperature dependence of the critical current density as obtained from kink temperatures in Fig. 2(a). To determine the screening current induced by a magnetic field in a thin-film ring, we use a formula derived by Brandt [Eq. (14) in Ref. 12]: $I=\pi RH/[\ln(8R/w)-0.5]$, where R is the mean radius of the ring, w the width of the ring, and H the applied field. For the ring geometry used in the present study, this yields a current of I (A)=1.55 H (mT) or a current density J (10^6 A/cm^2) =1.55 H (mT). For example, in 5 μT, the kink in M vs T in Fig. 2(a) occurs at 77 K. Thus, the critical current at 77 K is I_C=(1.55) (0.005) A=7.8 mA, corresponding to a critical current density J_C=7.8 kA/cm^2.

To determine the critical current of GBs in transport measurements, a voltage criterion of 1 μV is typically used. In our persistent-current measurements, the voltage drop across the GB is considerably less [we estimate it to be less than 10^{-12} V (see Ref. 11)]. It is thus desirable to directly compare the two methods on the same sample. For this purpose, six Au pads were evaporated on the ring of Fig. 2(a). The ring with the Au contacts was then heated to 380 °C for several hours (in flowing O_2) to ensure good electrical contacts. Electrical leads were then attached to the Au contacts by Ag paint cured at room temperature. A slit was cut into the ring in order to control the current flow [see inset in Fig. 2(b) (lower panel)]. The magnetization measurements of Fig. 2(a) were performed after the heat treatment for the Au contacts, i.e., between the magnetic and resistive measurements, the ring was not above room temperature at any time. This is important to ensure the same oxygen concentration for both the magnetic and transport measurements. By choosing the appropriate contacts for current and voltage leads, we were able to measure the current-voltage characteristics of both sections of the GB [see inset in Fig. 2(b)]. Figure 2(b) (lower panel) displays these I-V curves at 77 K. Using the 1 μV voltage criterion yields similar critical currents for the two junctions, 8.4 and 9.8 mA, and current densities [upper scale in Fig. 2(b)] of 8.4 and 9.8 kA/cm^2, respectively. From the magnetization measurements in Fig. 2(a), we obtain a critical current at 77 K of 7.8 kA/cm^2, which should be compared to the lower value obtained resistively, since flux penetration will first occur in the GB with the lowest J_C value. This close agreement between the two methods with widely different voltage criteria suggests that the I-V curves of the transport measurements are extremely steep with very little change in current over many orders of magnitude change in voltage.

The magnetization vs temperature curves in Fig. 2(a), at temperatures above the kink, reflect the decrease in GB critical current with increasing temperature at a given applied field. Figure 3 displays this critical current, as directly determined from the magnetization curves in Fig. 2(a) after the diamagnetic signal of the annulus was subtracted.[11] For a given applied field, the maximum measurable critical current occurs at the kink temperature since at $T<T_K$, the induced current is less than the critical current and the magnetization becomes temperature independent [Fig. 2(a)]. The maximum measurable critical current (observed with cooling) also depends on the applied field since the induced current is proportional to the applied field. As can be seen in Fig. 3, a

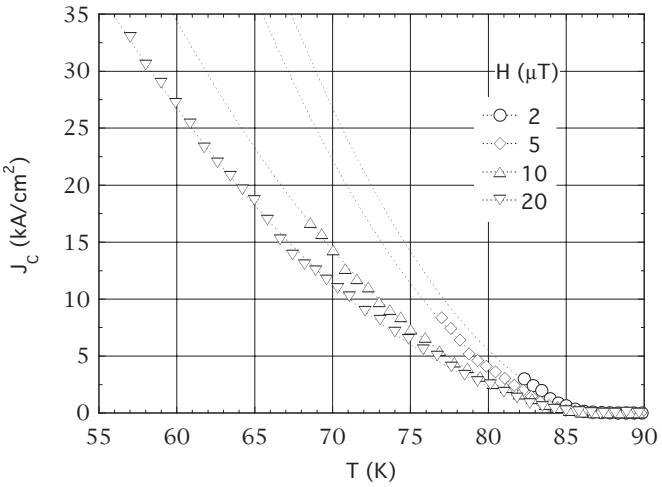

FIG. 3. Grain boundary critical current density, measured in various magnetic fields, for the same ring as used in Fig. 2. J_C was obtained from the data in Fig. 2(a) after subtracting the signal of the annulus, which is proportional to the applied field (see text). Measurements for the curves end at the kink temperatures [Fig. 2(a)] where the induced current becomes less than the critical current. The dashed lines are second order polynomial fits to the data (see text).

suppression of the critical current with increasing applied field is observed. Extrapolating second order polynomial fits to the data to 77 K yields a decrease in J_C at 77 K by about a factor of 2, relative to the zero-field limit, in a field of 20 μT.

The data in Fig. 2 clearly demonstrate that the magnetic measurements yield results very similar to the transport measurements. However, the ability to perform measurements without electrical contacts, as afforded by the magnetization technique, offers a great advantage over the resistive method for studying the effect of secondary heat treatments on GB supercurrent transport. The risk of sample damage from repeated contact placement is eliminated. Also, for small angle GBs where the critical current of the GB can be as large as 50 A at low temperatures in the geometry used, the magnetic method for the determination of critical currents is far preferable since transport measurements would require the patterning of a microbridge. This is a much more complicated and demanding procedure, especially for repeated oxygenation steps. Thus, for the remainder of this paper, we only report magnetization measurements for the determination of GB critical currents.

Figure 4(a) (upper panel) displays magnetization measurements from a ring containing a 10° GB. Here, the magnetization curves vary nearly linearly all the way to T_C. Here, no shoulder is seen in contrast to the ring with the 24° GB in Fig. 2(a). This indicates that for the ring containing the 10° GB, the critical current of the GB near T_C is comparable with that of the film material (see below). Also, in contrast to the 24° GB (Fig. 3), no suppression of the critical current by the measured fields is observed, i.e., at $T > T_K$, M vs T is almost a universal curve, independent of the magnetic fields applied during the measurement.

Figure 4(b) (lower panel) shows the magnetization curves for a single crystal film without any GB. Here, no sharp kink

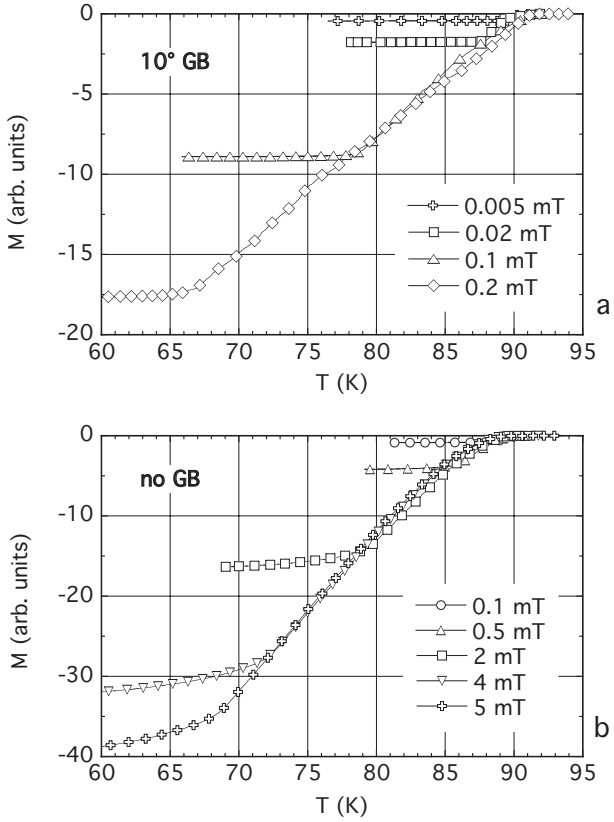

FIG. 4. Magnetization vs temperature in various applied magnetic fields as indicated. The data were obtained on warming after initially cooling in zero field to low temperatures. (a) (Upper panel): For a ring containing a 10° GB. (b) (Lower panel): For an epitaxial ring with no GB.

is observed when the flux starts penetrating into the bore of the ring. At low temperature, the induced shielding current flows only near the outer rim of the ring. As the temperature increases, the current is spread over a wider and wider part of the ring, i.e., the Bean profile penetrates deeper and deeper into the ring.[11] This causes the magnetic moment $M = \pi R^2 I$ (R the average radius of the current loop) to decrease slightly at constant induced current because R is decreasing. At the temperature where the Bean profile reaches the inner rim of the ring and the shielding current is uniformly distributed over the width of the ring, the flux starts penetrating into the bore.[9] Above this temperature, the persistent current flowing around the ring is no longer constant but is limited by the critical current, which decreases almost linearly with temperature independent of the magnetic field [for the small field values used in Fig. 4(b); see below for the effect of larger magnetic fields]. The onset of this linear $M(T)$ variation can be easily recognized in Fig. 4(b). At the temperature of this onset the current induced by the applied magnetic field equals the critical current of the ring.[9]

2. High critical current measurements

The highest field available in our SQUID magnetometer is 5 mT, which means that we can map the critical current of

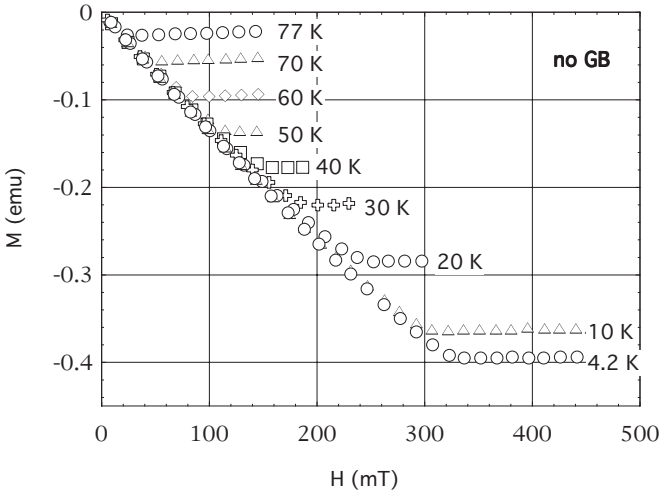

FIG. 5. Magnetization vs applied magnetic field at various temperatures as indicated. The data are for the same ring with no GB as used for Fig. 4(b). The data were obtained with increasing field after initially cooling in zero field from above T_C to various temperatures as indicated.

this ring down to only about 70 K [Fig. 4(b)]. To obtain critical current values at lower temperatures, we performed magnetization measurements in a VSM. Figure 5 shows such measurements for the same ring as that of Fig. 4(b). The ring was initially cooled to a given temperature in zero field. The magnetic moment was then monitored as the field was increased. With increasing field, the persistent current in the ring increases until the critical current is reached. At even higher fields, the persistent current flowing in the ring (and also the magnetic moment) remains constant at the critical value characteristic of the measurement temperature. From the field value at which the kink occurs, we can determine the current induced by this field in the same way as was done for the SQUID measurements. The results obtained with the SQUID magnetometer and the VSM agree very well in the overlapping field regime. Alternatively, we can determine the ring current from the magnetic moment $M=\pi R^2 I$. The latter values are about 20% lower than the ones obtained from the Brandt formula above. This relatively small difference could be due to the fact that the VSM was calibrated with a Ni cylinder rather than a thin-film ring. Also, the formula by Brandt used to calculate the induced current is an approximation for very narrow rings.[12] In the remainder of the paper, we use the Brandt formula to determine the critical current.

3. Summary: As-made films

Figure 6(a) shows critical current densities for selected rings with various GB angles as a function of temperature. The critical current density was determined with the Brandt formula above from measurements like those in Figs. 4 and 5. $J_C(T)$ for the single crystal ring varies from about 4×10^6 A/cm^2 at 77 K to about 5×10^7 A/cm^2 at the lowest temperature (4.2 K). For the 10° GB, J_C values are consistently about an order of magnitude smaller. Critical current densities for the 15° and 24° GBs continue to systematically decline with increasing misorientation angle. Below about

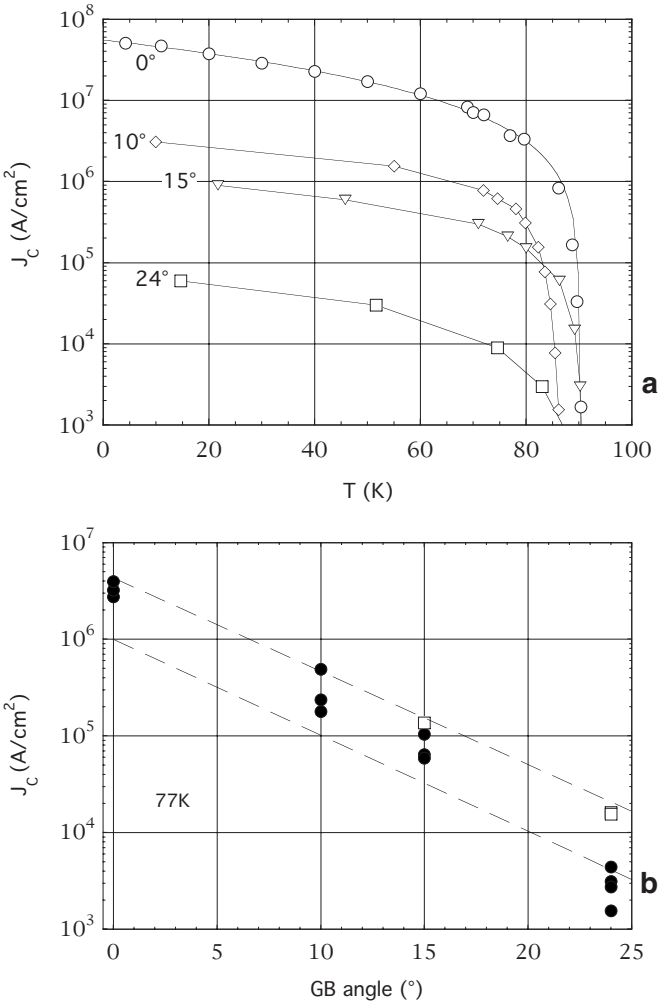

FIG. 6. (a) (Upper panel): Critical current densities vs temperature of selected rings, one ring containing no GB (0°) and rings with 10°, 15°, and 24° GBs, respectively. The data were obtained from measurements like those in Figs. 2(a), 4, and 5. (b) (Lower panel): Critical current density at 77 K vs GB angle for all rings investigated in the as-made state. Most published literature values lie in the region between the two dashed lines. The open squares are the critical current after secondary oxygenation (see text).

80 K, $\log(J_C)$ is approximately linear in temperature for all of the GBs; slopes for the $\log(J_C)$ vs T plots are comparable. The observed crossover above 80 K is a consequence of the different T_C values of the various films (see below). Figure 6(b) shows a plot of J_C at 77 K vs GB angle. At each angle, we have measured several rings. The values of J_C in Fig. 6(b) are well within the range of published values[17] for film samples most of which lie in the region between the two dashed lines in Fig. 6(b).

It is well known that there can be a wide variation in measured critical current densities across nominally identical GBs. The reason is not fully understood. Differences in impurity level and/or oxygen concentrations are suspected. For example, we investigated the critical current of four different rings all containing a 10° GB. The films were made by an identical procedure. Nevertheless, we observe a large variation in their critical current densities and significant variation

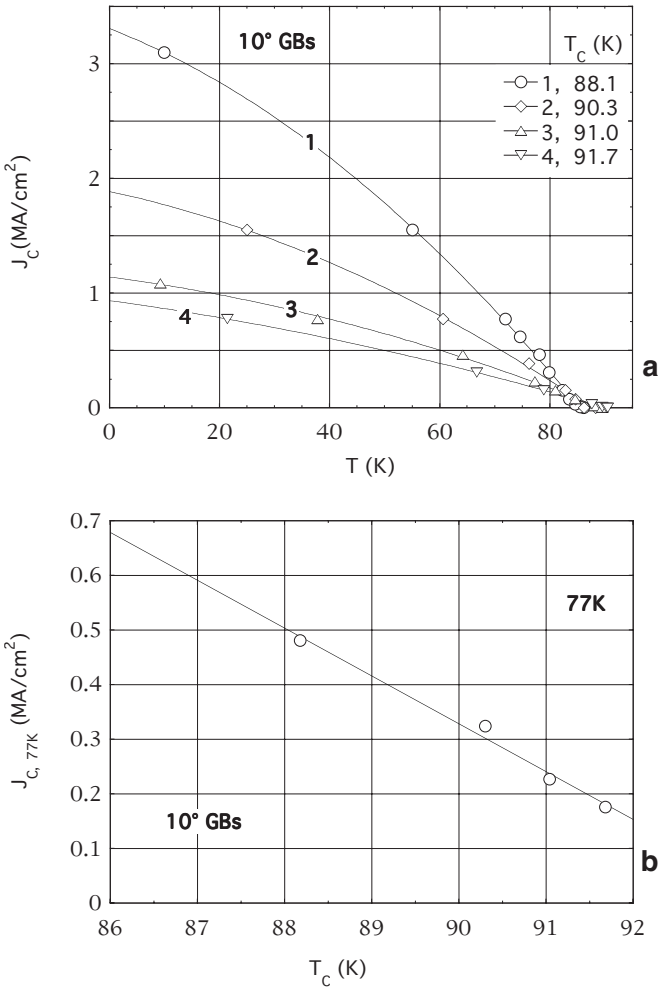

FIG. 7. Critical current densities of four rings each containing a 10° GB. (a) (Upper panel): Critical current density vs temperature. The superconducting transition temperature of each ring is listed next to the ring number. (b) (Lower panel): Critical current density at 77 K vs the superconducting transition temperature of each ring.

in their transition temperatures. Figure 7(a) (upper panel) displays the critical current for these four GBs as a function of temperature. At low temperatures, there is more than a factor of 3 difference between the strongest and weakest of the 10° GBs. We noticed a surprising correlation between J_C and T_C for these films. The film T_C is listed in Fig. 7(a) next to the sample number. The ring with the highest T_C has the lowest J_C value and vice versa. Figure 7(b) displays a plot of J_C at 77 K vs T_C. The monotonic behavior suggests that the films may contain different amounts of oxygen, with the highest oxygen concentration in the film with the lowest T_C (overdoped regime, see Fig. 1 and discussion below). The strong increase in J_C may then be due to an increasing level of oxygen doping in the GBs. A similar behavior, i.e., an increase of J_C with increasing doping level in the overdoped regime, has been previously observed for 24° bicrystal films of $Y_{1-x}Ca_xBa_2Cu_3O_{7-\delta}$ as function of Ca doping[6] and also for oxygen doping.[18] In the next section, we report the results of a systematic study investigating the effect of oxygen doping on the critical current density across GBs in thin-film samples.

B. Oxygen doping

1. Single crystal films

After the samples were investigated in the as-made state, they were subjected to various secondary oxygenation treatments, as described above. We first investigated a film ring without an artificial GB. This ring was prepared with our second method involving a Ag protective layer and sand blasting. We were mainly interested in the overdoped regime where T_C decreases again with increasing oxygen concentration. In a previous study on coated conductors, we have demonstrated that in this regime, J_C keeps on increasing with oxygen concentration despite the fact that T_C decreases again.[9] In an earlier investigation, Feenstra *et al.*[19] have also found a similar increase of J_C in the overdoped regime of epitaxial YBCO films. In that investigation, different films were fabricated for the various oxygen concentrations. Knowing that there can be significant variation in J_C of films with nominally the same oxygen concentration (see, for example, the results for Fig. 7 in this paper), it is preferable to use one film and vary its oxygen concentration.

Figure 8 (upper panel) shows the diamagnetic transition curves (in 1 μT) for one single crystal film ring after quenching from various oxygenation temperatures, as indicated. The highest T_C (optimal doping) is obtained after oxygenation at 475 °C. As the oxygenation temperature is reduced, T_C systematically decreases, as expected in the overdoped regime. The numbers labeling the curves indicate the sequence in which the experiments were performed, i.e., the 475 °C state was obtained first and the 400 °C state was obtained last (number 5). Figure 8 (lower panel) displays the J_C (T) curves corresponding to the various oxygenation states. The data were obtained from measurements like those shown in Figs. 4 and 5. The results are very similar to those obtained for coated conductors.[9] Below about 80 K, J_C systematically increases with increasing oxygen concentration (decreasing oxygenation temperatures) despite the fact that T_C decreases significantly. Figure 9 shows J_C as a function of the oxygenation temperature (approximate oxygen concentration on upper scale) for various measuring temperatures on a logarithmic scale (open symbols, left scale). The variation of the oxygen concentration with the oxygenation temperature was estimated by comparing the present results to those previously obtained on YBCO single crystals. There, the oxygen concentration was determined by neutron scattering.[20]

Also shown in Fig. 9 is T_C (solid symbols, right scale) obtained from the curves in Fig. 8 (upper panel) by linear extrapolation of the near-vertical parts of the transition curves to zero (onset temperatures). Except for the highest temperatures, J_C monotonically increases with increasing oxygen concentration, whereas T_C monotonically decreases. The fact that both T_C and J_C vary systematically with the oxygenation temperature, despite the more or less random sequence of the oxygenation procedures (see Fig. 8, upper panel), clearly indicates the reversible nature of the oxygenation process. The behavior for the single crystal film observed here is very similar to the results obtained by Feenstra *et al.*[19] and also to those previously obtained by Claus *et al.*

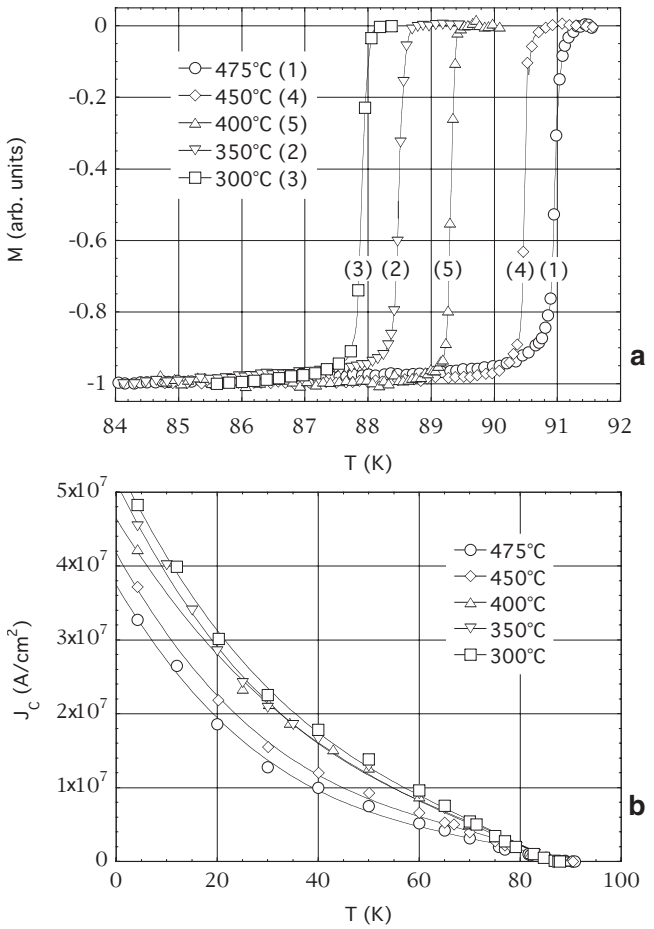

FIG. 8. (a) (Upper panel): Diamagnetic transition in 1 μT of a YBCO film ring in states of various oxygen concentrations (oxygenation temperatures). The numbers labeling the curves refer to the sequence in which the oxygenation treatments were performed (see text). (b) (Lower panel): Critical current densities of the film ring in the same states as in (a). J_C was determined from measurements like those shown in Figs. 4 and 5 (see text).

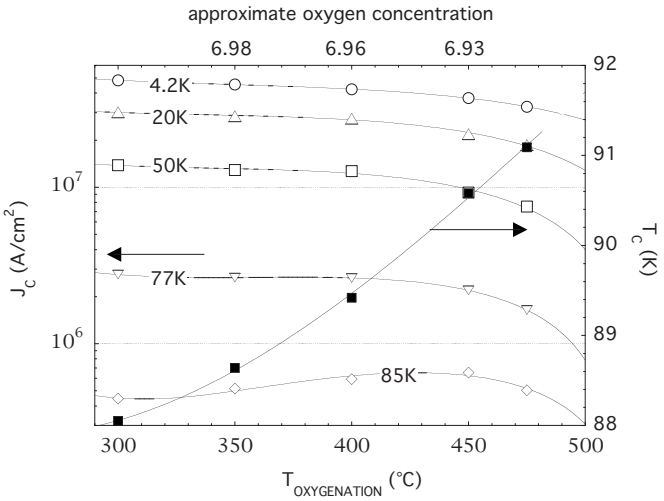

FIG. 9. Critical current density (open symbols, left scale) of the YBCO thin-film ring at various absolute temperatures (numbers labeling curves) as a function of the oxygenation temperature (lower scale). The upper scale indicates approximate oxygen concentrations (see text). Also shown is the transition temperature (solid squares, right scale). The data were obtained from the measurements shown in Fig. 8 (see text).

for coated conductors.[9] In a related experiment, Oates *et al.* recently showed that oxygen overdoping of YBCO films significantly lowered nonlinear effects in their microwave surface impedance.[21]

The general rule for type-II superconductors is that the pinning strength and the critical current increase the further one is away in temperature from T_C. This is not the case for YBCO films in the overdoped regime. Here, J_C increases despite the fact that T_C decreases. Feenstra *et al.* attributed this behavior to a monotonic dependence of the vortex pinning energy on the charge carrier density.[19] It has been shown from specific heat measurements that the superconducting condensate monotonically increases with increasing oxygen concentration from the underdoped to the well overdoped regime.[20] It has been suggested that this is due to the linear Cu-O chains, which participate in the superconductivity in the overdoped regime.[20] This increase in condensate could be responsible for the observed increase in J_C. Additionally, as a consequence of the chains becoming superconducting, the superconducting state becomes more three dimensional which, in turn, increases the pinning strength of the vortices (see, for example, Ref. 22).

2. Films with GBs

We now turn to the effect the oxygen concentration has on the critical current of GBs. Figure 10 (upper panel) displays the magnetization in 5 μT of a thin-film ring bisected by a 24° GB. Data are shown for the as-made ring and for the same ring after a 3 day anneal at 400 °C in flowing oxygen. (Subsequent experiments showed that much shorter oxygenation times are sufficient to achieve the equilibrium GB oxygen concentration at this temperature.) In the as-made state, the superconducting transition temperature T_C is 91.6 K (onset temperature). The kink temperature is about 64 K, i.e., the critical current at 64 K equals the induced shielding current in 5 μT which is 7.8 mA or 7.80 kA/cm^2. After the 400 °C oxygenation, T_C decreased by almost a degree to 90.8 K. The decline in T_C at this low oxygenation temperature suggests that the oxygen concentration of the film has increased (overdoped regime). However, the kink temperature has increased by almost 20 K. Thus, it appears that increasing the oxygen concentration significantly improves the critical current of the 24° GB.

Figure 10 (lower panel) shows the $J_C(T)$ determined from the kink temperatures for the same ring in three different oxygenation states. As the annealing temperature is decreased (oxygen level increased), dramatic increases in J_C are observed at all temperatures. The systematic decrease in T_C (T_C is listed in Fig. 10, lower panel, next to the oxygenation temperatures) with increased oxygen level demonstrates that the ring is in the overdoped regime. At 77 K, J_C for this GB increases by more than an order of magnitude with oxygen overdoping, relative to the as-made condition (near optimal doping). Another 24° GB that we investigated

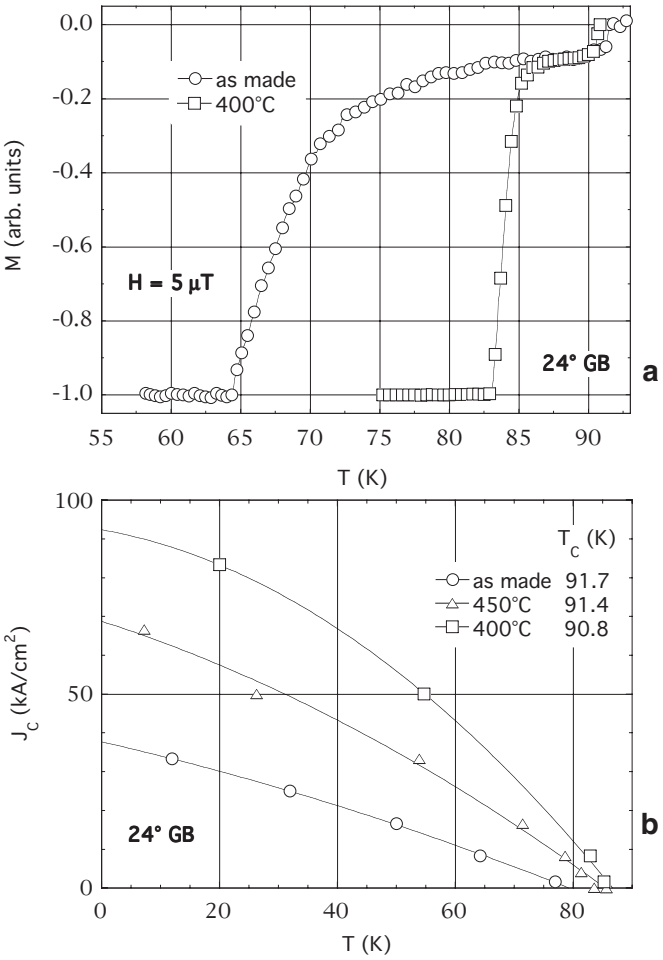

FIG. 10. Effect of oxygen doping of a 24° GB. (a) (Upper panel): Magnetization in 5 μT in the as-made state and after oxygenation at 400 °C. (b) (Lower panel): Critical current density of the same ring vs temperature in the as-made state and after oxygenation at 450 and 400 °C. The corresponding T_C values are listed next to the oxygenation temperature.

showed a smaller increase in J_C with overdoping (about a factor of 4 at 77 K).

We expect that annealing below 400 °C should further increase the oxygen concentration, resulting in lower T_C and even higher J_C values. This behavior was observed in thin-film ring samples made from coated conductors protected by a Ag layer.[9] These rings were made by dry etching (sand blasting). Their behavior is expected to closely resemble that of single crystal films. J_C was seen to systematically increase and T_C declined, even as annealing temperatures were reduced to 300 °C.[9] However, in the annealing studies of the photolithographically processed samples, sample degradation was encountered after several anneals, which resulted in irreversible decreases in J_C. It is possible that residues on the film left over from the photolithographic process caused this degradation when extended low-temperature annealing times were required. Thus, larger enhancements in the critical currents might be achievable by oxygen doping if this competing degradation could be avoided.

The temperature dependence of the critical current of the two 24° GBs in the as-made state (one shown in Figs. 2 and 3 and the other in Fig. 10) seem to be qualitatively different, with different signs of the curvature. The data displayed in Figs. 2 and 3 are mainly above 60 K, whereas in Fig. 10, the data are mainly below 60 K. In general, the temperature dependence of J_C changes curvature, being positive near T_C and negative at low temperature. The exact location of the inflection point is sample dependent.

For practical applications incorporating coated conductor technology, performance is generally limited by the presence of relatively small angle GBs (typically less than 10°). Thus, it is important to examine the behavior of GBs in the crossover regime where J_C becomes limited by GBs rather than bulk processes, as the GB misorientation is increased.

We thus extended the secondary oxygenation treatments to rings containing 15° and 10° GBs. Figure 11 shows the behavior of a ring with a 15° GB after oxygenation at various temperatures. Shown are magnetization measurements in a very small magnetic field of 1 μT (Fig. 11, upper panel). With increasing temperature, after initially cooling in zero field to low temperature, the M vs T curves display a kink signaling the start of flux penetration into the bore. At the kink temperature, the critical current of the GB equals the current induced by the 1 μT field. After a steep decrease in $M(T)$, the curves reach a plateau, indicating that J_C of the GB has decreased to zero. The remaining signal is due to the flux expulsion from the YBCO film annulus. This last remaining diamagnetism disappears at T_C of the film. As can be seen in Fig. 11 (upper panel), T_C decreases with increasing oxygen concentration (decreasing oxygenation temperature) from 91.9 K in the as-made state to 89.5 K after oxygenation at 350 °C. Also, the temperature interval right below T_C, where J_C of the GB remains zero, narrows considerably with oxygenation, just as for the 24° GB in Fig. 10. The critical-current vs temperature curves, corresponding to the various oxygenation states, are shown in Fig. 11 (lower panel). Except for a temperature interval near T_C, J_C increases with increasing oxygenation at all temperatures. Near T_C, the improvement, which would have resulted from the increased doping level, is overcompensated by the decrease in T_C, leading to the observed crossover.

The critical current of a 10° GB behaves very similar to that of the 15° boundary, as shown in Fig. 12. With increasing oxygenation level, T_C decreases by about the same amount as the T_C for the ring with the 15° GB (the T_C values are listed next to the oxygenation temperatures in Fig. 12). The ring used in Fig. 12 is the ring shown in Fig. 7 with the highest T_C value and lowest $J_C(T)$. After oxygenation at 350 °C, this ring had a T_C of 89.3 K (Fig. 12). According to Fig. 7, we would expect an increase of about a factor of 2 in J_C at 77 K. Instead, we hardly observe any increase of J_C at this temperature (Fig. 12). Comparing results at 40 K, we see that the increase of J_C observed for the 24° GB is about 4.5×10^4 A/cm^2, for the 15° GB, the increase is about 15×10^4 A/cm^2, and for the 10° boundary, the increase is about 40×10^4 A/cm^2. However, as the misorientation angle decreases, the percentage increase in J_C becomes considerably smaller than that observed for the 24° GB.

For all rings investigated, we observe some degradation of the GBs after repeated oxygenation steps. This could impact the quantitative changes that we observe. Future work

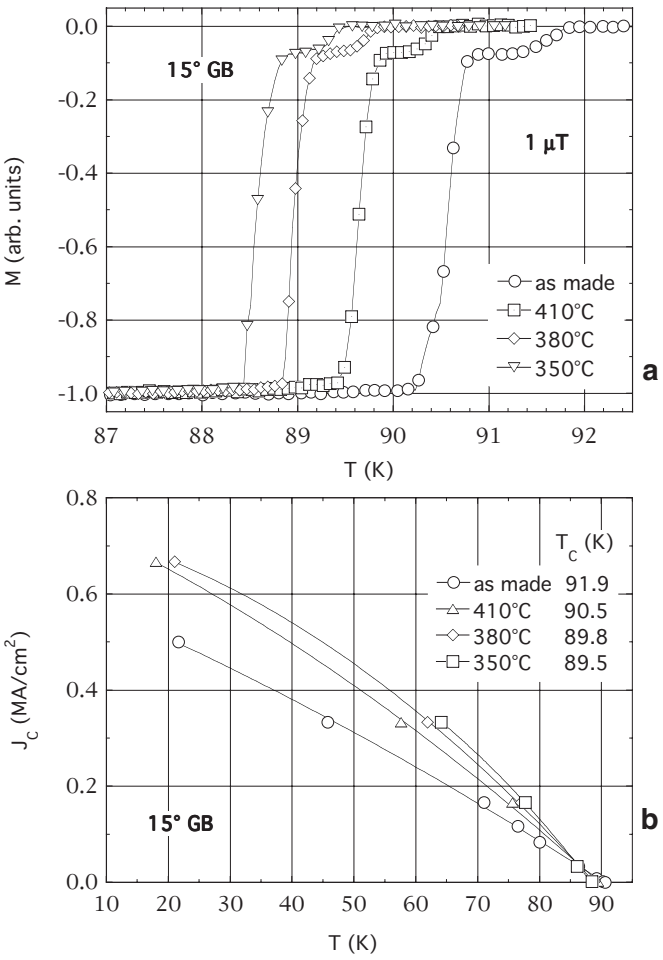

FIG. 11. Effect of oxygen doping of a 15° GB. (a) (Upper panel): Magnetization in 1 μT in the as-made state and after oxygenation at 410, 380, and 350 °C. This figure demonstrates how T_C is changing with oxygen concentration. (b) (Lower panel): Critical current density of the same ring vs temperature in the as-made state and after oxygenation at 410, 380, and 350 °C. The J_C data were obtained from measurements like those in Figs. 2, 4, and 5. The corresponding T_C values are listed next to the oxygenation temperature.

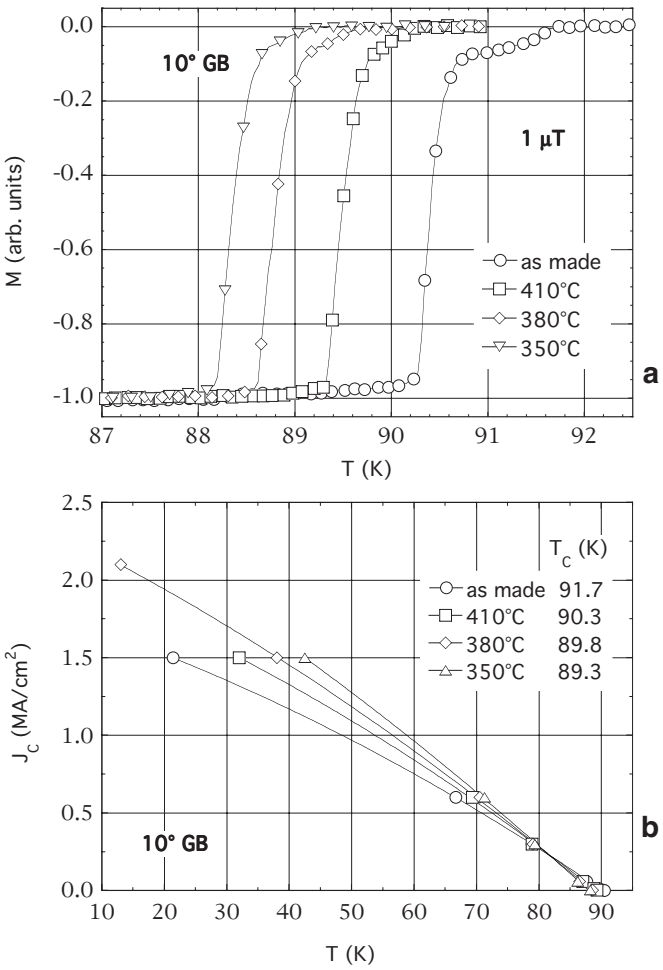

FIG. 12. Effect of oxygen doping of a 10° GB. (a) (Upper panel): Magnetization in 1 μT in the as-made state and after oxygenation at 410, 380, and 350 °C. (b) (Lower panel): Critical current density of the same ring vs temperature in the as-made state and after oxygenation at 410, 380, and 350 °C. The data were obtained from measurements like those in Figs. 2, 4, and 5. The corresponding T_C values are listed next to the oxygenation temperature.

with uncontaminated rings should clarify this problem.

C. Discussion

We have observed that when the oxygen content of a YBCO film bicrystal is increased, there is a remarkable increase in the critical current density across the GB. This is true when the sample is both underdoped and overdoped and holds for a wide range of GB (001) tilt misorientation angles. To understand this, we first note the common belief that vortices in high-angle GBs are Josephson vortices, which revert to Abrikosov vortices as GB angles become vanishingly small. Thus, for large angle GBs, flux transport through the GB occurs via Josephson vortices, and several models have been proposed to explain the GB J_C by the pinning of Josephson vortices.[23] For reasonably high fields, an important pinning mechanism can be the interaction with pinned Abrikosov vortices, which border the GB,[24,25] but this mechanism is ineffective for the present case of low fields. It is also argued that GB meandering in thin-film bicrystals, epitaxially grown on bicrystal substrates, occurs on a length scale that is favorable for pinning of Josephson vortices. While this mechanism is certainly operable, we have observed that GB pinning increases with oxygenation level in melt-textured bulk samples where GB meandering does not occur on a comparable length scale.[26] In addition, oxygenation is unlikely to change the GB pinning landscape, e.g., meandering, that involves the microstructure on the 100 nm length scale.[17,27] We thus rule out pinning as a cause, so a different mechanism is needed.

We have also observed that the J_C of single crystal YBCO films (no GBs) and bulk melt-textured samples[22] systematically increases as the oxygen content is increased (see also Ref. 9 for coated conductor films). For GB angles of 0°–15°, the relative increases in J_C after oxygenation are similar for GBs and epitaxial films, for the same changes in oxygen concentration (oxygenation temperature). The fact that the

doping dependence of our GBs (0°–15°) emulates that of epitaxial films, either by dc transport[19] or by rf techniques,[21] suggests a common origin. The Josephson critical current across GBs has three principal elements, the pinning of Josephson vortices along the boundary (that was ruled out above as a possible cause), the Josephson barrier transparency, and the strength of superconductivity in the grains neighboring the GB. The latter element reflects the fact that the Josephson J_C will tend to zero for a vanishing superconducting order parameter in the banks of the GB. That latter element is *not* the result of pinned Abrikosov vortices in the banks of the GB since Abrikosov vortices would only affect the *pinning* of Josephson vortices. Of these two remaining elements, the strength of superconductivity is the only one that is consistent with a common origin to epitaxial films. This is because the pinning effectiveness of defects for Abrikosov vortices also depends on the strength of superconductivity in the surrounding epitaxial film. The fact that the relative increases in J_C for GBs (angles of 0°–15°) and epitaxial films are similar indicates that barrier transparency is not primarily involved. However, it is important to point out that for large angle (e.g., 24°) grain boundaries, the enhancement of the GB J_C far exceeds the enhancement of epitaxial films, supporting the case for improved barrier transparency, as has been argued[6,7] for Ca doping of 24° GBs. Our data indicate that the enhancement of the barrier transparency with oxygenation occurs fairly abruptly with GB angle, somewhere between 15° and 24°. The enhancement of the barrier transmission by oxygenation is presumably possible in the higher-angle GBs because of their greater strain and/or natural defects.

IV. CONCLUSION

In conclusion, we observe significant increases in the grain boundary J_C after oxygen doping. This is especially apparent for the 24° GB at 77 K, where the J_C showed a tenfold increase with overdoping, compared to the J_C at optimal doping. For all GBs examined (10°, 15°, and 24°), oxygen overdoping increased the J_C relative to the optimally doped condition. However, while enhancements were always substantial at low temperatures, the enhancements were small at 77 K for the low angle boundaries. Thus, it appears that for both bulk transport and transport across GBs, the highest J_C is achieved at low temperatures ($T \ll T_C$) with maximum oxygen doping. However, since T_C is depressed with overdoping, operation at temperatures too close to T_C can result in a depressed J_C. It appears that this (latter) behavior occurs for small angle GBs, even at temperatures close to 77 K. This underscores the added value of oxygenation for improved J_C (with ~5 K drop in T_c), relative to Ca doping with its 10 K drop in T_c.

ACKNOWLEDGMENTS

Work at Argonne was supported by the U.S. Department of Energy, Basic Energy Sciences, Materials Sciences and the Office of Energy Efficiency and Renewable Energy, as part of a DOE program to develop power technology, under Contract No. DE-AC02-06CH11357. Work at Los Alamos was supported by the U.S. Department of Energy, Office of Energy Efficiency and Renewable Energy, as part of a DOE program to develop power technology, under Contract No. W-7405-ENG-36.

*Present address: College of DuPage, 425 Fawell Blvd., Glen Ellyn, IL 60137-6599.

[1] D. Dimos, P. Chaudhari, and J. Mannhart, Phys. Rev. B **41**, 4038 (1990).

[2] D. K. Finnemore, K. E. Gray, M. P. Maley, D. O. Welch, D. K. Christen, and D. M. Kroeger, Physica C **320**, 1 (1999).

[3] X. D. Wu, S. R. Foltyn, P. N. Arendt, W. R. Blumenthal, I. H. Campbell, J. D. Cotton, J. Y. Coulter, W. L. Hults, M. P. Maley, H. F. Safar, and J. L. Smith, Appl. Phys. Lett. **67**, 2397 (1995).

[4] A. Goyal, D. P. Norton, J. D. Budai, M. Paranthaman, E. D. Specht, D. M. Kroeger, D. K. Christen, Q. He, B. Saffian, F. A. List, D. F. Lee, P. M. Martin, C. E. Klabunde, E. Hatfield, and V. K. Sikka, Appl. Phys. Lett. **69**, 1795 (1996).

[5] K. Hasegawa, N. Yoshida, K. Fujino, H. Mukai, K. Hayashi, K. Sato, S. Honjo, Y. Sato, T. Ohkuma, H. Ishii, Y. Iwata, and T. Hara, *Advances in Superconductivity IX: Proceedings of the 9th International Symposium on Superconductivity*, October 21–24, 1996, Sapporo, Japan, edited by S. Nakajimaand M. Murakami (Springer, Berlin, 1997), p. 745; M. Bauer, R. Semerad, and H. Kinder, IEEE Trans. Appl. Supercond. **9**, 1502 (1999).

[6] A. Schmehl, B. Goetz, R. R. Schulz, C. W. Schneider, H. Bielefeldt, H. Hilgenkamp, and J. Manhart, Europhys. Lett. **47**, 110 (1999).

[7] G. Hammerl, A. Schmehl, R. R. Schulz, B. Goetz, H. Bielefeldt, C. W. Schneider, H. Hilgenkamp, and J. Manhart, Nature (London) **407**, 162 (2000).

[8] Part of this work was published in the *Proceedings of the Sixth European Conference on Applied Superconductivity, Sorrento, Italy, 14–18 September 2003*, [Inst. Phys. Conf. Ser. 181, 93 (2004)].

[9] H. Claus, K. K. Uprety, B. Ma, A. P. Paulikas, V. K. Vlasko-Vlasov, U. Welp, B. W. Veal, and K. E. Gray, Physica C **416**, 1 (2004).

[10] B. Ma, M. Li, R. E. Koritala, B. L. Fisher, A. R. Markowitz, R. A. Erck, R. Baurceanu, S. E. Dorris, D. J. Miller, and U. Balachandran, Supercond. Sci. Technol. **16**, 464 (2003).

[11] H. Claus, U. Welp, H. Zheng, L. Chen, A. P. Paulikas, B. W. Veal, K. E. Gray, and G. W. Crabtree, Phys. Rev. B **64**, 144507 (2001).

[12] Th. Herzog, H. A. Radovan, P. Zieman, and E. H. Brandt, Phys. Rev. B **56**, 2871 (1997).

[13] H. Darhmaoui and J. Jung, Phys. Rev. B **53**, 14621 (1996).

[14] J. R. Thompson, H. J. Kim, C. Cantoni, D. K. Christen, R. Feenstra, and D. T. Verebelyi, Phys. Rev. B **69**, 104509 (2004).

[15] The single crystal data are from our earlier work. See for example, R. Liu, B. W. Veal, A. P. Paulikas, J. W. Downey, H. Shi, C. G. Olson, C. Gu, A. J. Arko, and J. J. Joyce, Phys. Rev. B **45**, 5614 (1992); H. Zheng, M. Jiang, B. W. Veal, H. Claus, and B.

Obst, Physica C **301**, 147 (1998).
[16] J. D. Jorgensen, B. W. Veal, A. P. Paulikas, L. J. Nowicki, G. W. Crabtree, H. Claus, and W. K. Kwok, Phys. Rev. B **41**, 1863 (1990).
[17] See, for example, K. E. Gray, M. B. Field, and D. J. Miller, Phys. Rev. B **58**, 9543 (1998).
[18] B. Goetz, Ph.D. thesis, University of Augsburg, Germany, 2000.
[19] R. Feenstra, D. K. Christen, C. E. Klabunde, and J. D. Budai, Phys. Rev. B **45**, 7555 (1992).
[20] V. Breit, P. Schweiss, R. Hauff, H. Wühl, H. Claus, H. Rietschel, A. Erb, and G. Müller, Phys. Rev. B **52**, R15727 (1995).
[21] D. E. Oates, S. H. Park, M. A. Hein, P. J. Hirst, and R. G. Humphreys, IEEE Trans. Appl. Supercond. **13**, 311 (2003).
[22] D. H. Kim, K. E. Gray, R. T. Kampwirth, J. C. Smith, D. S. Richeson, T. J. Marks, J. H. Kang, J. Talvacchio, and M. Eddy, Physica C **177**, 431 (1991).
[23] D. J. Miller, K. E. Gray, M. B. Field, and DongHo Kim, IEEE Trans. Appl. Supercond. **9**, 2030 (1999).
[24] A. Gurevich and L. D. Cooley, Phys. Rev. B **50**, 13563 (1994).
[25] A. Gurevich, M. S. Rzchowski, G. Daniels, S. Patnaik, B. M. Hinaus, F. Carillo, F. Tafuri, and D. C. Larbalestier, Phys. Rev. Lett. **88**, 097001 (2002).
[26] B. W. Veal, H. Zheng, H. Claus, L. Chen, A. P. Paulikas, A. Koshelev, and G. W. Crabtree, Proceedings of the International Workshop on Superconductivity, Shimane, Japan, 19–22 June 2000 (unpublished), p. 211.
[27] Xiao-Feng Zhang, V. Todt, and Dean J. Miller, J. Mater. Res. **12**, 3029 (1997).